

# CHEMISTRY

## A European Journal

A Journal of



### Accepted Article

**Title:** Preparation of robust metal-free magnetic nanoemulsions encapsulating low-molecular-weight nitroxide radicals and hydrophobic drugs directed toward MRI-visible targeted delivery

**Authors:** Rui Tamura, Kota Nagura, Yusa Takemoto, Satori Moronaga, Yoshiaki Uchida, Satoshi Shimono, Akihiko Shiino, Kenji Tanigaki, Tsukuru Amano, Fumi Yoshino, Yohei Noda, Satoshi Koizumi, Naoki Komatsu, Tatsuhisa Kato, and Jun Yamauchi

This manuscript has been accepted after peer review and appears as an Accepted Article online prior to editing, proofing, and formal publication of the final Version of Record (VoR). This work is currently citable by using the Digital Object Identifier (DOI) given below. The VoR will be published online in Early View as soon as possible and may be different to this Accepted Article as a result of editing. Readers should obtain the VoR from the journal website shown below when it is published to ensure accuracy of information. The authors are responsible for the content of this Accepted Article.

**To be cited as:** *Chem. Eur. J.* 10.1002/chem.201702785

**Link to VoR:** <http://dx.doi.org/10.1002/chem.201702785>

Supported by  
**ACES**

WILEY-VCH

# Preparation of robust metal-free magnetic nanoemulsions encapsulating low-molecular-weight nitroxide radicals and hydrophobic drugs directed toward MRI-visible targeted delivery

Kota Nagura,<sup>[a]</sup> Yusa Takemoto,<sup>[a]</sup> Satori Moronaga,<sup>[a]</sup> Yoshiaki Uchida,<sup>[b,c]</sup> Satoshi Shimono,<sup>[a]</sup> Akihiko Shiino,<sup>[d]</sup> Kenji Tanigaki,<sup>[e]</sup> Tsukuru Amano,<sup>[f]</sup> Fumi Yoshino,<sup>[f]</sup> Yohei Noda,<sup>[g]</sup> Satoshi Koizumi,<sup>[g]</sup> Naoki Komatsu,<sup>[a]</sup> Tatsuhisa Kato,<sup>[a]</sup> Jun Yamauchi,<sup>[a]</sup> and Rui Tamura\*<sup>[a]</sup>

**Abstract:** With a view to developing a theranostic nanomedicine for magnetic resonance (MR) imaging-visible targeted drug delivery system, robust metal-free magnetic nanoemulsions (mean particle sizes of less than 20 nm) consisting of the biocompatible surfactant **1** and the incorporated hydrophobic low-molecular-weight 2,2,5-trimethyl-5-(4-alkoxy)phenylpyrrolidine-*N*-oxyl radicals [(±)-**2**] have been prepared in pH 7.4 phosphate-buffered saline. The structure of the nanoemulsions has been characterized by electron paramagnetic resonance spectroscopy, and dynamic light scattering and small angle neutron scattering measurements. The nanoemulsions showed high colloidal stability, low cytotoxicity, enough reduction resistance to excess ascorbic acid, and sufficient contrast enhancement in the proton longitudinal relaxation time ( $T_1$ )-weighted MR images in PBS *in vitro* and preliminarily *in vivo*. Furthermore, additional hydrophobic paclitaxel (**7**), an anticancer drug, could simultaneously be encapsulated inside the nanoparticles, and the resulting **7**-loaded nanoemulsions were efficiently incorporated into HeLa cells to suppress the cell growth.

## Introduction

Magnetic nanoparticles have attracted tremendous interest, particularly in biomedical applications, such as drug delivery system (DDS), hyperthermia therapy, and contrast enhancement for magnetic resonance imaging (MRI).<sup>[1-3]</sup> The majority of nanoparticles used are superparamagnetic iron oxides (magnetite  $\text{Fe}_3\text{O}_4$  or maghemite  $\gamma\text{Fe}_2\text{O}_3$ ) or iron-iron oxide core-shell, which are coated by a variety of polymeric or monomeric materials to prevent aggregation and sedimentation of the nanoparticles.<sup>[4-13]</sup> Practically these iron-containing nanoparticles, which are utilized as ferrofluids comprising magnetic colloidal particles (particle size < 100 nm) dispersed in a carrier fluid, can act as  $T_2$ -enhancing MRI contrast or hyperthermia therapy agents.<sup>[4-13]</sup> To employ these magnetic nanoparticles as drug delivery carriers, various drug molecules were attached to the biocompatible polymers, silica layers, or phospholipid bilayers coated on the magnetic core.<sup>[4-8]</sup> The use of such magnetic nanoparticles enables the simultaneous delivery and detection of therapeutic agents *in vivo*. However, there are some drawbacks associated with iron oxide-based contrast agents, because they demonstrated unusual magnetic susceptibility artifacts which produce dark signals that may not only be misleading but also result in an incorrect interpretation of the  $T_2$ -weighted MR images.<sup>[3]</sup>

Meanwhile, as biocompatible high-performance metal-free magnetic nanoparticles, a core-shell type of organic radical nanoparticles have been fabricated to be used as MRI and electron paramagnetic resonance imaging (EPRI) probes *in vivo*.<sup>[14-16]</sup> They comprised a self-assembling amphiphilic copolymers with stable nitroxide radical groups covalently bonded to the hydrophobic segment and showed high resistance to bioreduction. In the case of these polymeric nanoparticles, specific requirements such as degradability and accurate molecular weight as well as nontoxicity and biocompatibility must be satisfied.<sup>[7]</sup> As another example of metal-free magnetic nanoparticles, low-toxic, lyotropic mesophase (hexagonal-phase) nanoparticles (hexosomes) composed of amphiphilic glycerol monooleate and nitroxide lipids were employed as MRI contrast agents.<sup>[18,19]</sup> However, these mean particle sizes are much larger than those (10 to 100 nm) required for MRI contrast agents which are optimal for intravenous injection and have the most prolonged blood circulation time.<sup>[6]</sup> In this context, branched-bottlebrush copolymer nanoparticles with hydrodynamic diameters ranged from 13 to 24 nm and large polypropylenimine-scaffolded dendrimer molecules, both of which contain spirocyclohexyl nitroxide polyradicals, were reported to show excellent stability towards biological reducing agents and substantial *in vivo* MRI contrast.<sup>[20,21]</sup> However, thus far these metal-free nanoparticles have not possessed the function of DDS carriers.

- [a] K. Nagura, Y. Takemoto, S. Moronaga, Dr. S. Shimono, Prof. N. Komatsu, Prof. T. Kato, Prof. J. Yamauchi, Prof. R. Tamura  
Graduate School of Human and Environmental Studies  
Kyoto University, Yoshida Nihonmatsu-cho, Sakyo-ku, Kyoto 606-8501 (Japan)  
E-mail: tamura.rui.8c@kyoto-u.ac.jp
- [b] Prof. Y. Uchida  
Graduate School of Engineering Science  
Osaka University, Toyonaka, Osaka 560-8531 (Japan)
- [c] Prof. Y. Uchida  
PRESTO (Japan) Science and Technology Agency  
Kawaguchi, Saitama 332-0012, (Japan)
- [d] Prof. A. Shiino  
Biomedical MR Science Center  
Shiga University of Medical Science, Seta, Otsu 520-2192 (Japan)
- [e] Dr. K. Tanigaki  
Shiga Medical Center Research Institute  
Moriyama 5-4-30, Shiga 524-8524 (Japan)
- [f] T. Amano, F. Yoshino  
Department of Obstetrics and Gynecology  
Shiga University of Medical Science, Seta, Otsu 520-2192 (Japan)
- [g] Dr. Y. Noda, Prof. S. Koizumi  
Institute of Quantum Beam Science  
Ibaraki University, Ibaraki 316-8511 (Japan)

Supporting information for this article is given via a link at the end of the document.

## FULL PAPER

With these situation in mind, we have envisaged that if stable and biocompatible oil-in-water (O/W) nanoemulsions with appropriate particle sizes of 10 to 100 nm which can encapsulate large amounts of low-molecular-weight nitroxide radical molecules and show high resistance to bioreduction are easily available, these radical nanoparticles are most likely to be used as  $T_1$ -enhancing MRI contrast agents and EPRI probes *in vivo*. Furthermore, if hydrophobic drugs are incorporated into the same magnetic nanoemulsions, they may be employed as the drug carrier for MRI-visible targeted delivery system *in vivo*.

In this context, we reported that chiral all-organic rod-like liquid crystalline compounds with a stable five-membered cyclic nitroxide unit in the central core position exhibited a sort of spin glass-like inhomogeneous ferromagnetic interactions (the average spin-spin exchange interaction constant  $\bar{J} > 0$ ) induced by application of low magnetic fields in the LC phases at high temperatures (30–150 °C).<sup>[22–26]</sup> By EPR spectroscopic studies and DFT calculations, such a unique magnetic phenomenon, which was referred to as ‘positive magneto-LC effect’, was correlated with the preferential occurrence of ferromagnetic spin-spin dipole interactions in magnetic fields by a spin polarization mechanism due to the inhomogeneous intermolecular contacts through CH/ $\pi$  and/or CH/O interactions between the neighboring cyclic nitroxide radical moieties.<sup>[27]</sup> Furthermore, as the extension of such a unique magnetic phenomenon to another organic radical soft material system, we could prepare stable nitroxide radical liquid microcapsules (300  $\mu\text{m}$   $\phi$ ) consisting of monodispersed core-shell water-in-oil-in-water (W/O/W) double emulsion droplets.<sup>[28]</sup> These emulsions were magnetically transportable and served as a flexible antioxidative magnetic carrier for on-demand cargo transport systems and droplet-based sensors.

Here we report that the desired robust nanoemulsions consisting of equimolar amounts of the biocompatible non-ionic surfactant polyoxyethylene(20) cetyl ether **1** [Brij<sup>®</sup>58, C<sub>16</sub>H<sub>33</sub>(OCH<sub>2</sub>CH<sub>2</sub>)<sub>20</sub>OH]<sup>[29–31]</sup> and the incorporated low-molecular-weight 2,2,5-trimethyl-5-(4-alkoxyphenyl)pyrrolidine-N-oxyl radical [( $\pm$ )-**2**] were easily obtained without adding any stabilizer and that additional hydrophobic drugs could simultaneously be incorporated into the nanoemulsions (Chart 1a). Furthermore, these magnetic nanoemulsions exhibited sufficient contrast enhancement in the proton longitudinal relaxation time ( $T_1$ )-weighted MR images in (–)-PBS *in vitro* and preliminarily *in vivo*.

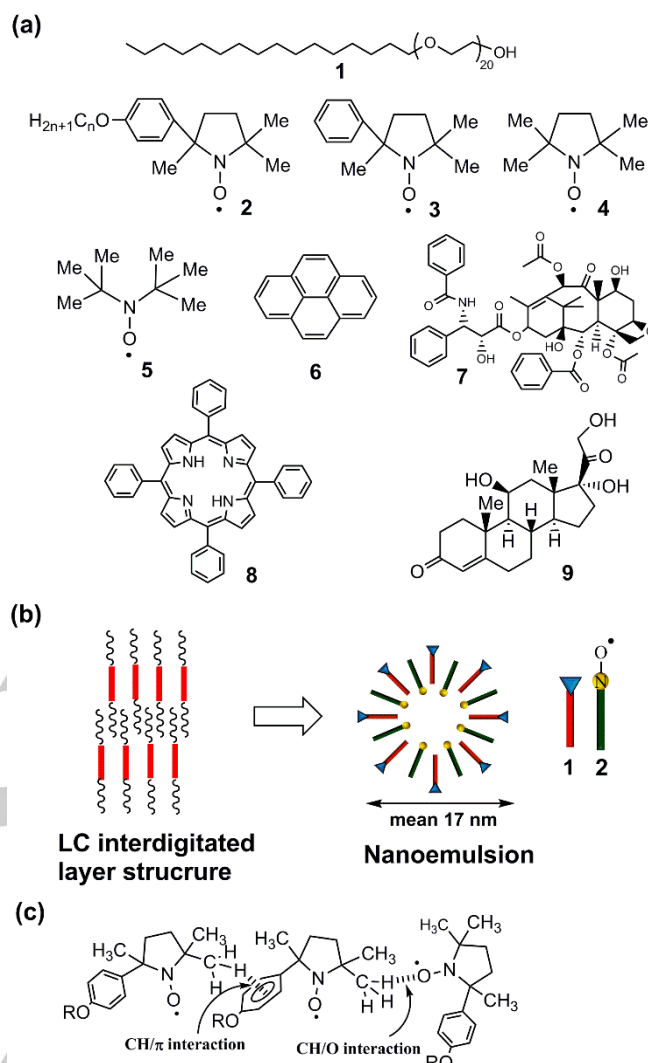


**Chart 1.** (a) Molecular structures used in this work: non-ionic surfactant **1**, nitroxide radicals **2**, 2,2,5-trimethyl-5-phenylpyrrolidinyloxy (**3**), 2,2,5,5-tetramethylpyrrolidinyloxy (**4**), di-*tert*-butyl nitroxide (**5**), pyrene (**6**), paclitaxel (**7**), tetraphenylporphyrin (**8**), and hydrocortisone (**9**). (b) Expected interdigitated layer structure in the nanoemulsion consisting of equimolar amounts of **1** and ( $\pm$ )-**2**. (c) Possible CH/ $\pi$  and CH/O interactions between the neighboring cyclic nitroxide radical moieties inside the nanoemulsion. See SI for the synthesis of ( $\pm$ )-**2**.

## Results and Discussion

### Preparation and characterization of magnetic nanoemulsions

Referring to the smectic liquid crystalline (LC) layer structure stabilized by interdigitated long alkyl chains, together with intermolecular CH/ $\pi$  and/or CH/O interactions (Chart 1b and c), the best combination of surfactant **1** (CMC: 0.007 to 0.077 mM) bearing a terminal C16 alkyl chain and nitroxides ( $\pm$ )-**2** with a long alkyl chain ( $n = 14$  to 20) or nitroxides ( $\pm$ )-**3–5** with no alkyl chain for comparison was searched to obtain most stable nanoemulsions with a mean particle size of less than 100 nm.

## FULL PAPER

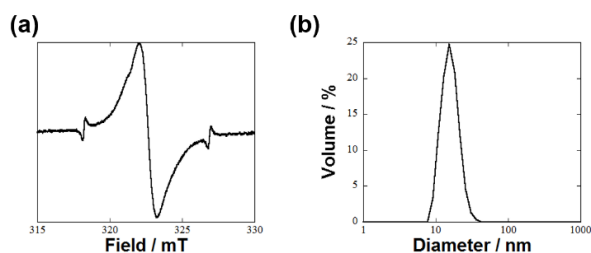


**Figure 1.** Characterization of the nanoemulsions prepared from equimolar amounts of **1** and ( $\pm$ )-**2** ( $n = 18$ ) (final concentration: 10 mM each) in PBS. (a) EPR spectrum of the sample filled in a capillary with the internal standard  $Mn^{2+}$  and (b) mean particle size (17 nm) determined by DLS measurement. See SI for the experimental detail.

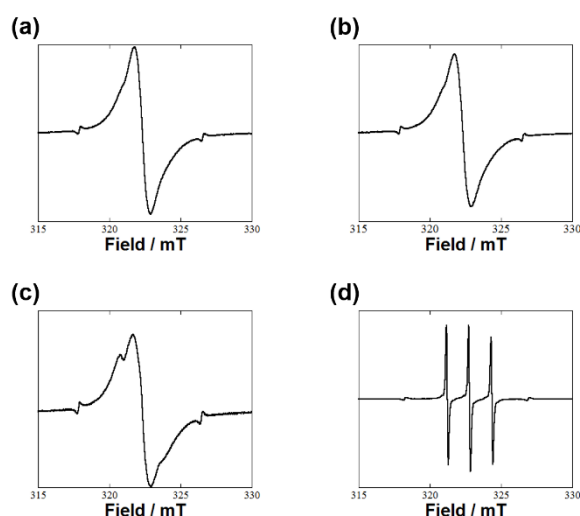


**Figure 2.** EPR spectra of the nanoemulsions immediately after preparation from equimolar amounts of **1** and ( $\pm$ )-**2** (final concentration: 10 mM each) in PBS with the internal standard  $Mn^{2+}$ . (a) ( $\pm$ )-**2** ( $n = 14$ ), (b) ( $\pm$ )-**2** ( $n = 16$ ), (c) ( $\pm$ )-**2** ( $n = 20$ ), and (d) ( $\pm$ )-**3**.

To a solution of **1** (10 mM) in pH 7.4 phosphate-buffered saline (PBS) was added an equimolar amount of solid ( $\pm$ )-**2** or oily ( $\pm$ )-**3**<sup>32</sup> dissolved in a minimum amount of ether, and the mixture was subjected to sonication (Branson Model 2510, power 125 W, frequency 42 KHz) for 3 min at 25 °C to give a white suspension or an oily mixture, respectively. Then the mixture was heated for more than 10 min at 90 °C to produce ether-free transparent nanoemulsions which were passed through a 0.45  $\mu$ m membrane filter (See SI for the experimental detail). The resulting nanoemulsions showed a beautiful Tyndall scattering upon irradiation of a visible laser light. In contrast, fairly water-soluble **4** and **5** failed to form emulsions. The stability and mean particle size of the resulting nanoemulsions encapsulating ( $\pm$ )-**2** or ( $\pm$ )-**3** were evaluated by electron paramagnetic resonance (EPR) spectroscopy and dynamic light scattering (DLS) measurement in PBS. A broad singlet EPR signal due to the self-assembly of nitroxide radical molecules within the nanoparticles was observed for the nanoemulsions containing water-insoluble ( $\pm$ )-**2** ( $n = 14, 16, 18$  or 20) (Figure 1a and 2a-c). In contrast, the mixed spectrum of a major three-line shape due to the free nitroxide radical molecules and the minor broad singlet signal arising from molecular aggregation was seen for fairly water-soluble ( $\pm$ )-**3** (Figure 2d).

**Table 1.** The mean particle sizes of the magnetic nanoemulsions composed of **1** and ( $\pm$ )-**2** ( $n = 14, 16, 18$  or 20) in PBS after 2 days from preparation at 25 °C.

( $\pm$ )- <b>2</b>	$n=14$	$n=16$	$n=18$	$n=20$
Particle size (nm)	55	26	17	18

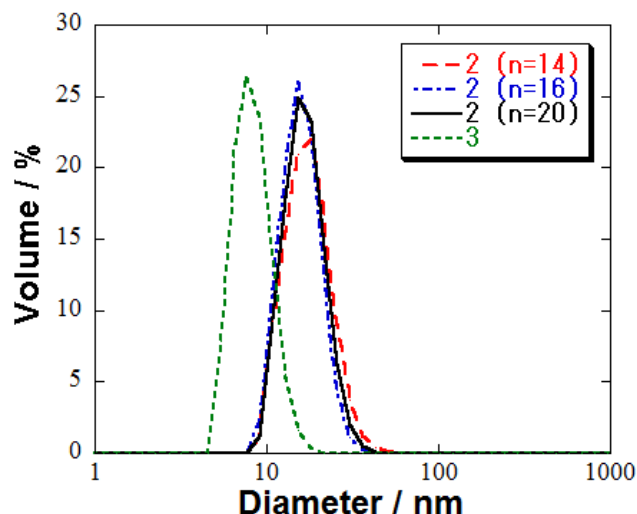


**Figure 3.** Mean particle sizes determined by DLS measurement of the nanoemulsions immediately after preparation from equimolar amounts of **1** and ( $\pm$ )-**2** (final concentration: 10 mM each) in PBS. ( $\pm$ )-**2** ( $n = 14$ ) (red dashed line), ( $\pm$ )-**2** ( $n = 16$ ) (blue dashed-dotted line), ( $\pm$ )-**2** ( $n = 20$ ) (black solid line), and ( $\pm$ )-**3** (green dotted line).

The nanoemulsions encapsulating hydrophobic ( $\pm$ )-**2** ( $n = 18$  or 20) showed outstanding stability; these mean particle sizes of 17 nm (in the range of 9–36 nm) or 18 nm (in the range of 8–30 nm) in PBS, respectively, were constant for more than two months at 12 °C (Figure 1b and 3, and Table 1). In contrast, the micelle solution (10 mmol) of **1** alone in PBS was unstable, giving a white precipitate after 2 days at 12 °C. The mean particle size (17 nm) of the nanoemulsions of ( $\pm$ )-**2** ( $n = 18$ ) with CMC of less than 0.01 mM was supported by small angle neutron scattering (SANS) measurement in  $D_2O$ ; the SANS profile observed at iMATERIA (BL20, J-PARC) was in good agreement with the scattering function for spherical particles and the particle radius was estimated to be  $6.0 \pm 2.0$  nm (Figure 4 and for the detail, see SI). In contrast, the nanoemulsions of ( $\pm$ )-**2** ( $n = 14$  or 16) disappeared after 6 or 10 days to give a white suspension, respectively (Figure 3 and Table 1). Based on the mean diameter (9 nm) of the micelle of **1** and the molecular length (3.3 nm) of **2** ( $n = 18$ ) which was calculated by the Molecular Mechanics using MM2 force field, the mean particle size (17 nm) for the nanoemulsions of ( $\pm$ )-**2** ( $n = 18$ ) indicates that both the flexible interdigitated layer structure of long alkyl chains and the  $CH/\pi$  and/or  $CH/O$  interactions between neighboring cyclic nitroxide radical moieties should greatly contribute to the remarkable stability of the nanoemulsions (Chart 1b and c). Furthermore, the nanoemulsions of ( $\pm$ )-**2** ( $n = 18$  or 20) were also stable after the 1000 times dilution (to 0.01 mM) with PBS. Thus, the nanoemulsions of **1** and ( $\pm$ )-**2** ( $n = 18$  or 20) turned out to be the best choice for biomedical application. For further experiment, ( $\pm$ )-**2** ( $n = 18$ ) with the less molecular weight was used. Meanwhile, the use of homologous non-ionic surfactants such as Brij®C10 [ $C_{16}H_{33}(OCH_2CH_2)_{10}OH$ ] and Brij®35 [ $C_{12}H_{25}(OCH_2CH_2)_{23}OH$ ] failed to prepare stable nanoemulsions encapsulating ( $\pm$ )-**2** ( $n = 14, 16, 18$  or 20) in the concentration of

## FULL PAPER

10 mM each in PBS, due most likely to the too short polyethylene glycol or alkyl chain length of the surfactants, respectively.

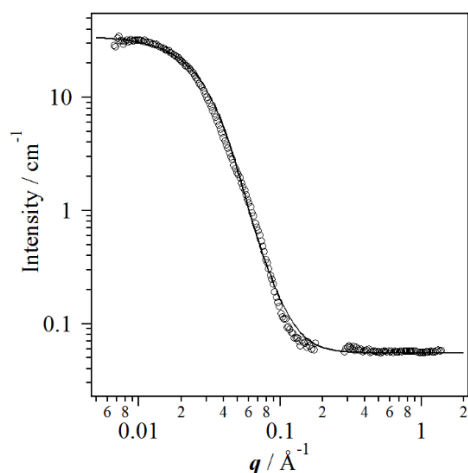


**Figure 4.** SANS profile of the nanoemulsion of **1** and  $(\pm)$ -**2** ( $n = 18$ ) in  $D_2O$ . The open circles were experimentally obtained. The solid line indicates the calculated profile assuming spherical particles with radius  $R = 6.0 \pm 2.0$  nm. See SI for the experimental detail.

### Reduction resistance to ascorbic acid

It is well known that water-soluble nitroxide radicals are readily reduced by antioxidants such as ascorbic acid (VC) and glutathione (GSH) *in vivo* to give the corresponding hydroxylamines.<sup>[14-16]</sup> Therefore, the reduction resistance of the nanoemulsions of **1** and  $(\pm)$ -**2** ( $n = 18$ ) (each final concentration: 10 mM) was evaluated in the presence of excess VC (final concentration: 17.5 mM) in PBS at 25 °C and compared with the experimental result using the same concentration of water-soluble 4-hydroxy-2,2,6,6-tetramethyl-1-piperidinyloxy (TEMPOL).<sup>[14-16]</sup> The decay of the spectral intensity for  $(\pm)$ -**2** ( $n = 18$ ) in response to VC was monitored by EPR spectroscopy (Figure 5). The nanoemulsions showed increased reduction resistance (half-life: 40 min) compared with TEMPOL (half-life: < 1 min); in fact we could not track the decay of EPR spectral intensity for TEMPOL due to the too fast reduction with VC. These results indicate that the nitroxyl groups are shielded by surfactant **1**, but slow water exchange occurs between the inner and outer spheres of the nanoemulsion most likely because of the polar circumstances in the central pore surrounded by nitroxyl groups.

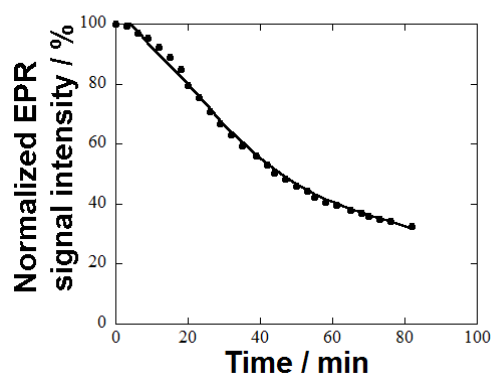


**Figure 5.** Resistance of  $(\pm)$ -**2** ( $n = 18$ ) in nanoemulsions to VC reduction. The reduction in the spectral intensity in PBS was monitored by EPR spectroscopy using a double integration method. See SI for the experimental detail.

### DDS carrier ability

To evaluate the ability of a DDS carrier, the magnetic nanoemulsions incorporating a hydrophobic quasi-drug pyrene (**6**) were prepared by adding a solution of one equiv of  $(\pm)$ -**2** ( $n=18$ ) and 10 mol% of **6** (based on the amount of **1**) in a small amount of ether to a PBS solution (10 mM) of **1**, followed by sonication and heating at 90 °C according to the prototypical procedure mentioned above. The resulting mean particle size was 17 nm, while that of the control nanoemulsions composed of **1** and **6** was 9.4 nm (Figure 6); these mean particle sizes were comparable to those of the nanoemulsions (17 nm) and the micelles (9 nm) in the absence of **6**. The incorporation of **6** into the nanoemulsions was confirmed by EPR, UV, and fluorescence spectroscopies; the fluorescence emission of **6** within the magnetic nanoemulsions was considerably quenched by the surrounding nitroxyl groups<sup>[20]</sup> and revived by adding a large excess (20 equiv based on the nitroxide molecules) of VC (Figure 7). These results support the interdigitated layer structure between alkyl chains of **1** and  $(\pm)$ -**2** (Chart 1b) in which molecules of **6** were intercalated.

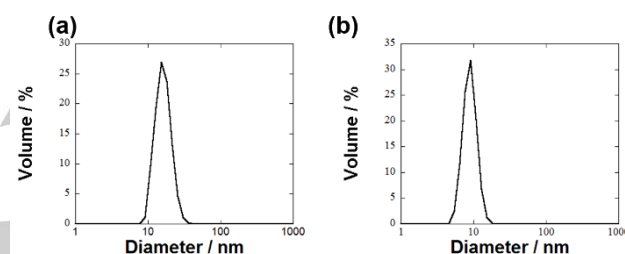


**Figure 6.** Determination of mean particle sizes (17 and 9.4 nm) of the nanoemulsions of **1** incorporating 10 mol% of **6** by DLS measurement immediately after preparation (a) in the presence of an equimolar amount of  $(\pm)$ -**2** ( $n=18$ ) based on **1** and (b) in the absence of  $(\pm)$ -**2**, respectively, in PBS.

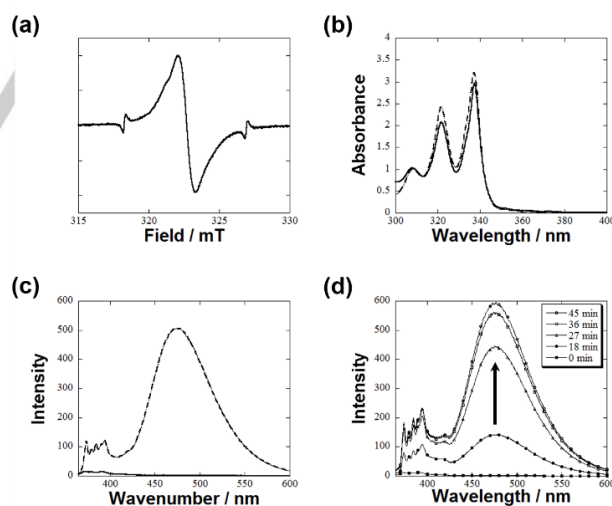


**Figure 7.** EPR, UV, and fluorescence spectra of the magnetic nanoemulsions encapsulating 10 mol% of **6** in PBS. (a) EPR spectrum of the **6**-loaded nanoemulsions of **1** and  $(\pm)$ -**2** ( $n=18$ ) with the internal standard  $Mn^{2+}$ , (b) UV spectra of the **6**-loaded nanoemulsions of **1** and  $(\pm)$ -**2** ( $n=18$ ) (solid line) and the **6**-loaded nanoemulsions of **1** (broken line), (c) fluorescent spectra of the **6**-loaded nanoemulsions of **1** and  $(\pm)$ -**2** ( $n=18$ ) and the **6**-loaded nanoemulsions of **1** (broken line), and (d) fluorescence spectral change in the **6**-loaded nanoemulsions of **1** and  $(\pm)$ -**2** after addition of 20 equiv of VC. See SI for the experimental detail.

Similarly, 10 mol% of hydrophobic drugs or quasi-drugs such as paclitaxel (Taxol®) (**7**), tetraphenylporphyrin (**8**) and

## FULL PAPER

hydrocortisone (**9**) were successfully incorporated into the magnetic nanoparticles by an analogous procedure. The mean particle size of the nanoemulsions encapsulating **7** was 12 nm by DLS measurement, while that incorporating **8** or **9** was 16 nm (Figure 8 d-f). Furthermore, the EPR spectrum of **7**-loaded nanoemulsions was a broad three-line shape, whereas **8** or **9**-loaded ones showed a broad singlet signal (Figure 8a-c). It was noticeable that the former exhibited the spectrum of a dispersed nitroxide radical in solution in contrast to the latter ones of self-assembled radicals. These results suggest that the bulky **7** bearing hydrogen-bond donating NH and OH groups should reside in the central position of nanoemulsions and interact with neighboring nitroxyl groups by hydrogen bond to form a quasi-solution, resulting in i) the formation of a deeply interdigitated layer structure between alkyl chains so as to decrease the mean diameter of the nanoemulsions and ii) a considerably slow rotation of the nitroxyl groups, both of which are advantageous to enlarge the MRI contrast ability as described later. In contrast, the nanoemulsions incorporating **8** or **9** with a fairly planar molecular structure would take an intercalated molecular assembly in the interdigitated layer, similar to the case of **6**-loaded ones.

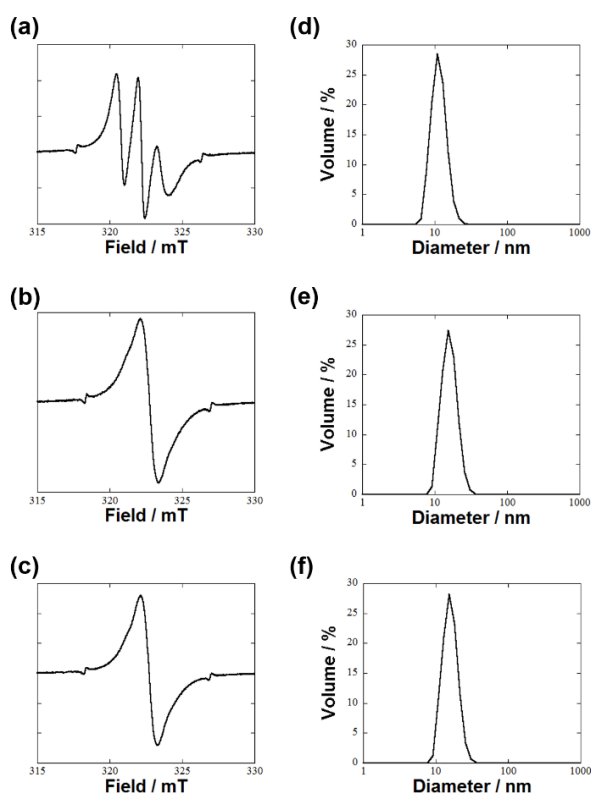


**Figure 8.** (a-c) EPR spectra with the internal standard  $Mn^{2+}$  and (d-f) mean particle sizes determined by DLS measurement immediately after preparation of the nanoemulsions of **1** and ( $\pm$ )-**2** ( $n=18$ ) encapsulating 10 mol% of (a, d) **7**, (b, e) **8**, and (c, f) **9** in PBS.

### In vitro cytotoxicity

To verify the uptake of the nanoemulsions into cancer cells, HeLa cells ( $9.0 \times 10^3$  cells in 100  $\mu$ L per well) cultured in a 96-well dish with Dulbecco's modified Eagle's medium (DMEM) containing 10% fetal bovine serum and 1% penicillin/streptomycin were treated with a PBS solution (10  $\mu$ L) of the micelles of **1**, the **7**-unloaded or loaded nanoemulsions composed of **1** and ( $\pm$ )-**2** ( $n=18$ ), or free **7** (Figure 9). The initial solution of the nanoemulsions containing 10 mM of **1** and ( $\pm$ )-**2** ( $n=18$ ) and as

low as 10  $\mu$ M of **7** was diluted with PBS by 1/8 [final concentration of **1** and ( $\pm$ )-**2** ( $n=18$ ): 1.25 mM each], 1/16 (0.625 mM), 1/32 (0.313 mM), 1/64 (0.156 mM), 1/128 (0.078 mM) and 1/256 (0.039 mM) before incubation. After incubation for 24 h at 37  $^{\circ}$ C under 5%  $CO_2$ , cells were washed with PBS twice and the cytotoxicity was evaluated by Cell Counting Kit-8 (CCK-8) assay. Consequently, both the micelles and **7**-unloaded nanoemulsions showed high toxicity in the concentrations of 0.625 mM (1/16 dilution) or higher, while they exhibited much lower or little toxicity in the concentration of 0.313 mM (1/32) or lower (Figure 9a). In contrast, both the **7**-loaded nanoemulsions and free **7** displayed significant toxicity against HeLa cells in the concentration of 0.156  $\mu$ M (1/64 dilution) or higher of **7**. Thus, the fact that the drug **7** released from the nanoemulsions is pharmaceutically active suggests that **7**-loaded nanoemulsions were incorporated into the cancer cells and are useful as a DDS drug carrier.

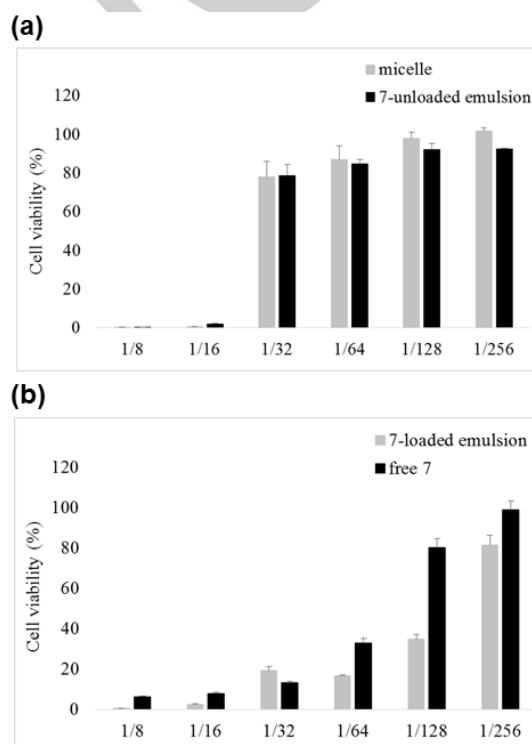


**Figure 9.** Evaluation of *in vitro* cytotoxicity of **7**-loaded magnetic nanoemulsions. HeLa cells in a culture medium were treated with a PBS solution of (a) the micelles of **1** and the **7**-unloaded nanoemulsions composed of **1** and ( $\pm$ )-**2** ( $n=18$ ), and (b) the **7**-loaded nanoemulsions and free **7**. The initial solution of the nanoemulsions containing 10 mM of **1** and ( $\pm$ )-**2** ( $n=18$ ) and 10  $\mu$ M of **7** was diluted with PBS by 1/8, 1/16, 1/32, 1/64, 1/128 and 1/256 before incubation; the final concentrations of **1** and ( $\pm$ )-**2** ( $n=18$ ) were 1.25, 0.625, 0.313, 0.156, 0.078 and 0.039 mM, while those of **7** were 1.25, 0.625, 0.313, 0.156, 0.078 and 0.039  $\mu$ M, respectively. The cell viability was assayed using CCK-8 kit after incubation for 24 h at 37  $^{\circ}$ C. See SI for the experimental detail.

### MRI measurement

The water proton relaxivity of the magnetic nanoemulsions containing 1.25 to 10 mM of **1** and ( $\pm$ )-**2** ( $n=18$ ) in PBS was evaluated on an MRI machine at 4.7 T (Figure 10a, A-D). The nanoemulsions prepared from the 10 mM (final concentration) solution of **1** and ( $\pm$ )-**2** ( $n=18$ ) significantly brightened the  $T_1$ -weighted MR phantom images compared with PBS alone (Figure 10a, L). Furthermore, we could observe the bright MR phantom images of the magnetic nanoemulsions incorporating 10 mol% of quasi-drugs **6** and **8** (Figure 10a, I and J) or drugs **7** and **9** (Figure 10a, E and K). Particularly, the **7**-loaded nanoemulsions exhibited

## FULL PAPER

the brightest contrast among them including the 7-unloaded nanoemulsions (Figure 10a, E). This is likely associated with the decrease in the mean particle size (12 nm) and the unique EPR spectrum as described in the previous section (Figure 8a and d), which allows relatively fast water exchange between the inner and outer spheres of the nanoemulsions and the increase in rotational correlation constant of nitroxyl groups.<sup>[18,19]</sup>

To evaluate the relaxation rate enhancement by the nitroxide-based magnetic nanoemulsions, the longitudinal relaxation rate ( $r_1$ ) was determined from the relaxation times as a function of concentration by using spin-echo method at 4.7 T with respect to the 7-unloaded and loaded nanoemulsions; linear regression analysis yielded the  $r_1$  of 0.12 and 0.16  $\text{mM}^{-1}\text{s}^{-1}$ , respectively (Figure 10 b and c). These  $r_1$  values were less than that (4.0  $\text{mM}^{-1}\text{s}^{-1}$  at 4.7 T) of Magnevist® [one of Gd(III) complex agents] in deionized water,<sup>[33]</sup> but comparable or larger than those (in the order of 0.1  $\text{mM}^{-1}\text{s}^{-1}$  at 4.7 T) for ordinary water-soluble small mononitroxide molecules.<sup>[34]</sup> However, the fact that there is a good linear relation between the  $T_1$  contrast enhancement and the concentration of nitroxyl groups would increase the significance of our nanoemulsions for biomedical application.<sup>[21,35]</sup> Furthermore, it is a big advantage that nitroxide radicals can act as  $T_1$ -enhancing MRI contrast agents with much lower toxicity in comparison with the commonly used molecular Gd(III) complex agents.<sup>[36-40]</sup>

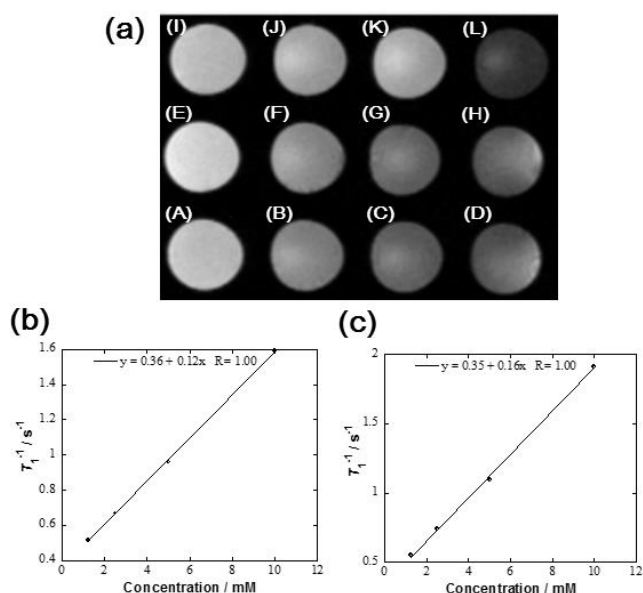


**Figure 10.**  $T_1$ -weighted MR phantom images of various magnetic nanoemulsions in PBS at 4.7 T and determination of the longitudinal relaxation rates ( $r_1$ ). (a) Panels (A-D) are the images of the magnetic nanoemulsions composed of equimolar amounts of **1** and ( $\pm$ )-**2** ( $n=18$ ) (final concentrations: 10, 5, 2.5 and 1.25 mM, respectively). Panels (E-H) are the images of the magnetic nanoemulsions composed of **1** and ( $\pm$ )-**2** ( $n=18$ ) (10, 5, 2.5 and 1.25 mM, respectively) encapsulating 10 mol% of **7**. Panels (I-K) are the images of the magnetic nanoemulsions composed of **1** and ( $\pm$ )-**2** ( $n=18$ ) (10 mM each) encapsulating 10 mol% of (I) **6**, (J) **8**, or (K) **9**. The control image of PBS alone is shown in panel (L). Plots of  $T_1^{-1}$  vs the concentration of ( $\pm$ )-**2** ( $n=18$ ) in (b) the 7-unloaded nanoemulsions and (c) the 7-loaded nanoemulsions; the  $r_1$  values were determined to be 0.12 and 0.16  $\text{mM}^{-1}\text{s}^{-1}$ , respectively. See SI for the experimental detail.

Finally, to examine whether the magnetic nanoemulsions can actually serve as an *in vivo* MRI contrast agent, a preliminary MRI experiment was performed using living mouse brain tissues. Three hundred microliter ( $\mu\text{L}$ ) of the nanoemulsions composed of **1** and ( $\pm$ )-**2** ( $n=18$ ) (10 mM each) in PBS were intravenously

injected into an anesthetized mouse (weight around 30 g) lying supinely in an animal holder. Subsequently, the cradle was inserted into the MRI machine (7.0 T) to acquire  $T_1$ -weighted MR images by the spin-echo method. Since it was anticipated that the injected nanoemulsions would be transported by the blood stream and accumulated to the pituitary gland in the brain,  $T_1$  weighted MR images of the pituitary gland were taken after the injection of the nanoemulsions. As a result, a distinct MRI contrast enhancement was observed in the pituitary gland after injection with high reproducibility (Figure 11 and S1). This result demonstrates that the nanoemulsions are effective as an *in vivo*  $T_1$ -shortening MRI contrast agent. Further detailed experiment to clarify where the magnetic nanoemulsions accumulate in healthy and tumor-bearing mice will be reported in due course.

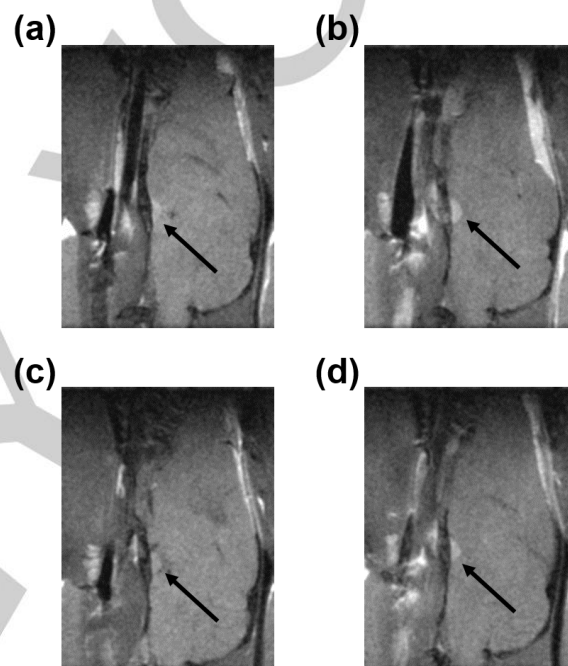


**Figure 11.**  $T_1$ -weighted MR images of brain tissues of two mice: (a, c) before and (b, d) 13 min after the intravenous injection of 300  $\mu\text{L}$  of the nanoemulsions composed of **1** and ( $\pm$ )-**2** ( $n=18$ ) (10 mM each) in PBS. The images in (a) and (b) correspond to one mouse, and those in (c) and (d) refer to the other mouse. Distinct contrast enhancement was observed in the pituitary glands of both mice (indicated by black arrows). See SI for the experimental detail.

## Conclusions

We have successfully prepared the ideal and robust, metal-free magnetic nanoemulsions with a desired mean particle size (17 nm) by simply heating a mixture of equimolar amounts of biocompatible non-ionic surfactant **1** and low-molecular weight nitroxide radical ( $\pm$ )-**2** ( $n=18$ ) at 90 °C in PBS, both of which possess long alkyl chains with similar length. The magnetic nanoemulsions exhibited high reduction resistance to ascorbic acid and sufficiently bright contrast in the proton  $T_1$ -weighted MR images *in vitro* and preliminarily *in vivo*, and incorporated as much as 10 mol % of hydrophobic drugs or quasi-drugs into the nanoparticles. From the cell viability assay, it has been concluded that the magnetic nanoemulsions show low toxicity in the concentrations (0.313 mM or lower) of **1** and ( $\pm$ )-**2** ( $n=18$ ) and that the anticancer drug 7-loaded nanoemulsions effectively suppress the HeLa cell growth in the concentrations of 0.078  $\mu\text{M}$  or higher of **7**. Thus, it is highly expected that these nanoemulsions will serve as a theranostic nanomedicine for MRI-visible targeted drug delivery system *in vivo*, if they have an additional function to be

## FULL PAPER

selectively incorporated and accumulated into the targeted cancer cells.

## Acknowledgements

The present work was supported by JSPS KAKENHI (Grant number 26248024). The neutron experiment at the Materials and Life Science Experimental Facility of the J-PARC was performed under a user program (Proposal No. 2016PM0005).

**Keywords:** Radicals • EPR spectroscopy • magnetic nanoparticles • imaging agents • drug delivery

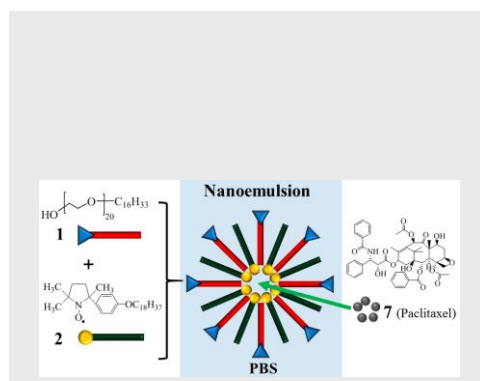
- [1] W. J. Stark, *Angew. Chem. Int. Ed.* **2011**, *50*, 1242-1258.
- [2] H. Goesmann, C. Feldmann, *Angew. Chem. Int. Ed.* **2010**, *49*, 1362-1395.
- [3] Magnetic Nanomaterials: Nanomaterials for the Life Sciences Vol. 4 (Ed. C. Kumar), Wiley-VCH, Weinheim, **2009**.
- [4] J. Huang, Y. li, Y.A. Orza, Q. Lu, P. Guo, L. Wang, L. Yang, H. Mao, *Adv. Funct. Mater.* **2016**, *26*, 3818-3836.
- [5] Z. Al-Ahmady, K. Kostarelos, *Chem. Rev.* **2016**, *116*, 3883-3918
- [6] S. Laurent, D. Forge, M. Port, A. Roch. C. Robic, L. V. Elst, R. N. Muller, *Chem. Rev.* **2008**, *108*, 2064-2110.
- [7] A-H. Lu, E. L. Salabas, F. Shüth, *Angew. Chem. Int. Ed.* **2007**, *46*, 1222-1244.
- [8] C. Corot, P. Robert, J-M. Idée, M. Port, *Adv. Drug Deliv. Rev.* **2006**, *58*, 1471-1504.
- [9] M. Piazza, M. Colombo, I. Zanoni, F. Granucci, P. Tortora, J. Weiss, T. Giannini, D. Prosperi, F. Peri, *Angew. Chem. Int. Ed.* **2011**, *50*, 622-626.
- [10] H. Chen, C. Deng, X. Zhang, *Angew. Chem. Int. Ed.* **2010**, *49*, 607-611.
- [11] L. Zao, T. Chano, S. Morikawa, Y. Saito, A. Shiino, S. Shimizu, T. Maeda, T. Irie, S. Aonuma, H. Okabe, T. Kimura, T. Inubushi, N. Komatsu, *Adv. Funct. Mater.* **2012**, *22*, 5107-5117.
- [12] G. Mikhaylov, U. Mikac, A. A. Magaeva, V. I. Itin, E. P. Naiden, I. Psakhye, L. Babes, T. Reinheckel, C. Peters, R. Zeiser, M. Bogyo, V. Turk, S. G. Psakhye, B. Turk, O. Vasiljeva, O. *Nature Nanotech.* **2011**, *6*, 594-602.
- [13] S. Cheong, P. Ferguson, K. W. Feindel, I. F. Hermans, P. T. Callaghan, C. Meyer, A. Slocombe, C-H. Su, F-Y. Cheng, C-S. Yeh, B. Ingham, M. F. Toney, R. D. Tilley, *Angew. Chem. Int. Ed.* **2011**, *50*, 4206-4209.
- [14] X. Zhuang, C. Xiao, K. Oyaizu, N. Chikushi, X. Chen, H. Nishide, *J. Poly. Sci. Part A: Polym. Chem.* **2010**, *48*, 5404-5410.
- [15] T. Yoshitomi, R. Suzuki, T. Mamiya, H. Matsui, A. Hirayama, Y. Nagasaki, *Bioconjugate Chem.* **2009**, *20*, 1792-1798.
- [16] T. Yoshitomi, D. Mikyamoto, Y. Nagasaki, *Biomacromolecules* **2009**, *10*, 596-601.
- [17] E. Soussan, S. Cassel, M. Blanzat, I. Rico-Lattes, *Angew. Chem. Int. Ed.* **2009**, *48*, 274-288.
- [18] N. Bye, O. E. Hutt, T. M. Hinton, D. P. Acharya, L. J. Waddington, B. A. Moffat, D. K. Wright, H. X. Wang, X. Mulet, B. W. Muir, *Langmuir* **2014**, *30*, 8898-8906.
- [19] B. W. Muir, D. P. Acharya, D. F. Kennedy, X. Mulet, R. A. Evans, S. M. Pereira, K. L. Wark, B. J. Boyd, T. Nguyen, T. M. Hinton, L. J. Waddington, N. Kirby, D. K. Wright, H. X. Wang, G. F. Egan, B. A. Moffat, *Biomaterials* **2012**, *33*, 2723-2733.
- [20] A. Sowers, J. R. McCombs, Y. Wang, J. T. Palette, S. W. Morton, E. C. Dreaden, M. D. Boska, M. F. Ottaviani, P. T. Hammond, A. Rajca, J. A. Johnson, *Nat. Commun.* **2014**, *5*, 5460.
- [21] A. Rajca, Y. Wang, M. Boska, J. T. Palette, A. Olankitwanit, M. A. Swanson, D. G. Mitchell, S. S. Eaton, G. R. Eaton, S. Rajca, *J. Am. Chem. Soc.* **2012**, *134*, 15724-15727.
- [22] Y. Uchida, K. Suzuki, R. Tamura, N. Ikuma, S. Shimono, Y. Noda, J. Yamauchi, *J. Am. Chem. Soc.* **2010**, *132*, 9746-9752.
- [23] K. Suzuki, Y. Uchida, R. Tamura, S. Shimono, J. Yamauchi, *J. Mater. Chem.* **2012**, *22*, 6799-6806.
- [24] Y. Uchida, K. Suzuki, R. Tamura, *J. Phys. Chem. B* **2012**, *116*, 9791-9795.
- [25] R. Tamura, Y. Uchida, K. Suzuki in *Handbook of Liquid Crystals: Second Edition* (Eds: J. W. Goodby, P. J. Collings, T. Kato. C. Tschierske, H. F. Gleeson, P. Raynes), Wiley-VCH, Weinheim, **2014**, vol. 8, pp. 837-864.
- [26] K. Suzuki, Y. Takemoto, S. Takaoka, K. Taguchi, Y. Uchida, D. G. Mazhukin, I. G. Grigor'ev, R. Tamura, *Chem. Commun.* **2016**, *52*, 3935-3938.
- [27] A. Kh. Vorobiev, N. A. Chumakova, D. A. Pomogailo, Y. Uchida, K. Suzuki, Y. Noda, R. Tamura, *J. Phys. Chem. B* **2014**, *118*, 1932-1042.
- [28] Y. Uchida, Y. Iwai, T. Akita, T. Mitome, K. Suzuki, R. Tamura, N. Nishiyama, *J. Mater. Chem. B* **2014**, *2*, 4130-4133.
- [29] J. Chamieh, F. Davanier, V. Jannin, F. Demarne, H. Cottet, *Inter. J. Pharm.* **2015**, *492*, 46-54.
- [30] L. Dupont-Leclercq, S. Giroux, B. Henry, P. Rubini, *Langmuir* **2007**, *23*, 10463-10470.
- [31] J. Schefer, R. McDaniel, B. Schoenborn, *J. Phys. Chem.* **1988**, *92*, 729-732.
- [32] K. Hideg, H. O. Hankovszky, H. A. Halasz, *J. Chem. Soc., Perkin Trans. 1* **1988**, 2905-2911.
- [33] L. Zhao, A. Shiino, H. Qin, T. Kimura, N. Komatsu, *J. Nanosci. Nanotechnol.* **2015**, *15*, 1076-1082.
- [34] K. Matsumoto, *Biol. Pharm. Bull.* **2009**, *32*, 711-716.
- [35] K. Matsumoto, H. Yakumaru, M. Narazaki, H. Nakagawa, K. Anzai, H. Ikehara, N. Ikota, *Magn. Reson. Imag.* **2008**, *26*, 117-121.
- [36] Bardelang, M. Hardy, O. Ouari, P. Tordo in *Encyclopedia of Radicals in Chemistry, Biology and Materials, Vol. 4 Polymers and Materials* (Eds: C. Chatgililoglu, A. Studer), John Wiley & Sons, Chichester, **2012**, pp. 1965-2015.
- [37] *Dynamic Contrast-Enhanced Magnetic Resonance Imaging in Oncology* (Eds.: A. Jackson, D. L. Buckley, G. J. M. Parker), Springer-Verlag, Berlin Heidelberg, **2005**.
- [38] Z. Zhelev, R. Bakalova, I. Aoki, K. Matsumoto, V. Gadjeva, K. Anzai, I. Kanno, *Chem. Commun.* **2009**, *45*, 53-55.
- [39] X. Wan, T. C. Fu, A. Funk, A.; R. E. London, *Brain Res. Bull.* **1995**, *36*, 91-96.
- [40] K. Matsumoto, M. Narazaki, H. Ikehira, K. Anzai, N. Ikota, *J. Magn. Reson.* **2007**, *187*, 155-162.

## FULL PAPER

## Entry for the Table of Contents (Please choose one layout)

## FULL PAPER

Metal-free magnetic nanoemulsions encapsulating hydrophobic drugs were prepared with a view to developing a theranostic nanomedicine for MRI-visible targeted drug delivery system.



K. Nagura, Y. Takemoto, S. Moronaga, Y. Uchida, S. Shimono, A. Shiino, K. Tanigaki, T. Amano, F. Yoshino, Y. Noda, S. Koizumi, N. Komatsu, T. Kato, J. Yamauchi, R. Tamura\*

Page No. – Page No.

**Preparation of robust metal-free magnetic nanoemulsions encapsulating low-molecular-weight nitroxide radicals and hydrophobic drugs directed toward MRI-visible targeted delivery**